Journal of Theoretical Biology 360 (2014) 67–77

Contents lists available at ScienceDirect

Journal of Theoretical Biology

journal homepage: www.elsevier.com/locate/yjtbi

Studying HIV latency by modeling the interaction between HIV proteins and the innate immune response

Luis U. Aguilera [a,b,1], Jesús Rodríguez-González [a,*]

[a] Centro de Investigacion y de Estudios Avanzados del IPN, Unidad Monterrey, Via del Conocimiento 201, Parque PIIT, CP 66600 Apodaca NL, Mexico
[b] University of Heidelberg, Im Neuenheimer Feld 267, 69120 Heidelberg, Germany

HIGHLIGHTS

- We model the behavior among HIV proteins and the innate immune response.
- Productive and latent cell phenotypes are described by bistable and bimodal dynamics.
- HIV latency is affected by the intensity of biochemical noise.
- HIV latency is affected by the strength of the innate immune response.

GRAPHICAL ABSTRACT

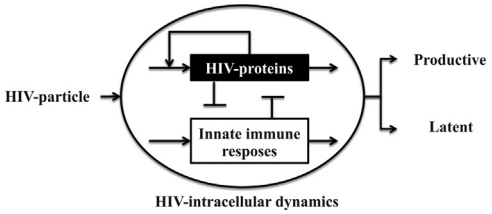

ARTICLE INFO

Article history:
Received 5 November 2013
Received in revised form
30 May 2014
Accepted 20 June 2014
Available online 2 July 2014

Keywords:
Restriction factor
Innate immune system
Tat circuit
Intracellular dynamics
Bistability

ABSTRACT

HIV infection leads to two cell fates, the viral productive state or viral latency (a reversible non-productive state). HIV latency is relevant because infected active CD4+ T-lymphocytes can reach a resting memory state in which the provirus remains silent for long periods of time. Despite experimental and theoretical efforts, the causal molecular mechanisms responsible for HIV latency are only partially understood. Studies have determined that HIV latency is influenced by the innate immune response carried out by cell restriction factors that inhibit the postintegration steps in the virus replication cycle. In this study, we present a mathematical study that combines deterministic and stochastic approaches to analyze the interactions between HIV proteins and the innate immune response. Using wide ranges of parameter values, we observed the following: (1) a phenomenological description of the viral productive and latent cell phenotypes is obtained by bistable and bimodal dynamics, (2) biochemical noise reduces the probability that an infected cell adopts the latent state, (3) the effects of the innate immune response enhance the HIV latency state, (4) the conditions of the cell before infection affect the latent phenotype, i.e., the existing expression of cell restriction factors propitiates HIV latency, and existing expression of HIV proteins reduces HIV latency.

1. Introduction

Highly active antiretroviral therapy (HAART) decreases viral loads during human immunodeficiency virus (HIV) infection and reduces clinical progression to acquired immunodeficiency syndrome (AIDS). Nevertheless, the long-term use of HAART cannot achieve viral clearance (Palmer et al., 2008; Williams and Greene, 2005). A major barrier to HIV eradication is the existence of a reservoir of resting memory CD4+ T-lymphocytes (T4 cells) carrying latent provirus (Chun et al., 1997).

HIV latency is the reversible non-productive infection of a cell (Abbas and Herbein, 2012; Marcello, 2006; Margolis, 2010). HIV latency is characterized by an integrated provirus that is replication competent but expresses no or not all viral gene products (Donahue and Wainberg, 2013).

* Corresponding author. Tel.: +52 81 11561740; fax: +52 81 11561741.
E-mail addresses: luis.aguilera@bioquant.uni-heidelberg.de (L.U. Aguilera), jrodriguez@cinvestav.mx (J. Rodríguez-González).
[1] Tel.: +49 6221 5451275; fax: +49 6221 54 51483.

http://dx.doi.org/10.1016/j.jtbi.2014.06.025
0022-5193/

The integrated HIV provirus acts as a transcription template that is regulated at the transcriptional and posttranscriptional levels (Karn and Stoltzfus, 2012). Regulation of HIV gene expression depends on the chromatin environment at the site of integration (Jordan et al., 2001; Verdin et al., 1993) and complex interactions between HIV regulatory proteins and the cellular machinery (Marcello, 2006).

The HIV Tat protein is a key component in HIV decision making. An HIV Tat-positive autoregulatory loop increases HIV gene expression 100-fold over basal expression levels (Nabel and Baltimore, 1987). The absence of the HIV Tat protein results in premature transcription termination (Jordan et al., 2001). Overexpression of the HIV Tat protein is sufficient to induce HIV gene expression (Donahue et al., 2012).

HIV intracellular dynamics are strongly affected by the randomness of discrete molecular events (Balázsi et al., 2011). Biochemical noise describes the randomness of molecular events (Adrews et al., 2009). Studies considering biochemical noise in HIV intracellular dynamics have proved that the transcriptional Tat circuit generates excitable dynamics (Konkoli and Jesorka, 2013; Razooky and Weinberger, 2011; Weinberger and Shenk, 2007; Weinberger et al., 2005).

The innate immune response inhibits steps in the HIV replication cycle, contributing to the modulation of HIV latency (Barr, 2010; Huang et al., 2007; Pan et al., 2013; Zack et al., 2013). Commonly, the inhibitory effects of the innate immune response are directly or indirectly antagonized by HIV proteins (Duggal and Emerman, 2012). Recent reports have theoretically studied the mutual negative interaction between the innate immune system and viral proteins describing the outcome of viral infection by deterministic dynamical behaviors that include monostability, bistability and oscillations (Tan et al., 2012; Zou et al., 2010).

In this paper, we used deterministic and stochastic methods to explore whether HIV latency can be explained by considering the interplay between the transcriptional Tat circuit and the mutual negative interactions between the innate immune response and HIV proteins.

2. Theory

2.1. Innate immune responses

Innate immune responses that interfere with HIV intracellular dynamics are caused by cell restriction factors (CRFs). CRFs are host cellular biomolecules that block specific stages of the HIV replication cycle (Duggal and Emerman, 2012). The expression of most CRFs is induced by interferon (IFN) (Barr, 2010). Among the experimentally validated CRFs that interfere with HIV transcription are Murr1 (Ganesh et al., 2003), ISG20 (Espert et al., 2005) and PKR (Sadler et al., 2009). CRFs that interfere in HIV translation are OAS1/RNAseL (Maitra and Silverman, 1998) and specific cellular microRNAs (Cojo et al., 2011; Sanghvi and Steel, 2012). CRFs that interfere during the HIV trafficking/budding steps are Tim22 (Barr et al., 2008), Tetherin/BST-2 (Perez-Caballero et al., 2009) and ISG15 (Okumura et al., 2006).

2.2. Counter restriction by HIV proteins

Some HIV proteins have evolved the ability to antagonize CRFs (Kirchhoff, 2010). Experimentally validated HIV counter inhibitors of CRF include Vpu, which inhibits Tetherin/BST-2 (Perez-Caballero et al., 2009), Tat, which inhibits microRNAs pathways (Cojo et al., 2011; Sanghvi and Steel, 2012) and OAS1/RNAseL (Schröder et al., 1990), and HIV antagonistic activity against ISG20 (Espert et al., 2005). Additionally, Vpu and Vif independently interfere with the transcription of IFN and hence inhibit the expression of IFN-induced genes through indirect mechanisms (Donahue and Wainberg, 2013).

2.3. HIV intracellular regulatory network

Like the negative mutual interactions between CRF and HIV proteins, HIV gene expression mechanisms generates a complex interaction network (Fig. 1A). In this network, HIV intracellular dynamics are determined by HIV gene expression (basal expression and Tat transactivation), the inhibitory effects of CRF in postintegration steps during the HIV replication cycle, and counter-inhibition of CRFs by HIV proteins.

3. Mathematical model of the HIV molecular interaction network

To develop the mathematical model of the HIV molecular interaction network given in Fig. 1A, we combined intermediate molecules and similar feedback loops to obtain an essential network circuit (Klipp et al., 2011). The obtained circuit is given in Fig. 1B. It summarizes how the complex regulatory network can be reduced into a model with two components, the HIV proteins (V) and the CRFs (C) in an HIV-infected cell. The main characteristics of this circuit are a positive feedback loop in V (basal expression and Tat transactivation) and mutual negative feedback loops

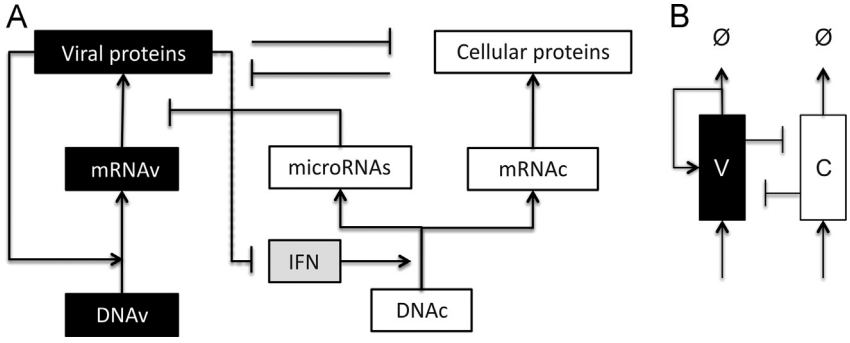

Fig. 1. (A) HIV intracellular regulatory network. First, we represent the mechanisms of HIV gene expression (production of mRNA and proteins). A self-positive feedback loop given by the HIV Tat protein enhances HIV gene expression. The expression mechanisms of cellular genes with antiviral activity (microRNAs and proteins) are also shown. CRF interference in HIV replication includes human microRNAs, Murr1, OAS1/RNAseL, Trim22, ISG15, ISG20 and Tetherin/BST-2. HIV proteins that antagonize CRF include Tat and Vpu proteins. Additionally, the HIV proteins Vif and Vpu inhibit the expression of IFN, resulting in the inhibition of the transcription of most cell proteins with antiviral activity. (B) A circuit that abstracts the essential structure of network A. Black boxes represent viral elements, and white boxes represent cellular elements. Arrows represent positive interactions, and lines with hammer ends represent negative interactions.

between V and C (the mutual negative interaction between the innate immune response and HIV proteins).

This model consists of the following two differential equations that account for the temporal evolution of the concentrations of V and C, respectively:

$$\dot{V} = k_{BV} + k_V(V/(V+k_M)) - k_{VC}VC - k_{dV}V, \quad (1)$$

$$\dot{C} = k_C - k_{CV}VC - k_{dC}C. \quad (2)$$

The meaning of the functions, variables and parameters in the above equations is as follows. Parameter k_{BV} represents the basal expression of V (Nabel and Baltimore, 1987). The Michaelis–Menten function $k_v(V/(V+k_M)$ denotes the transcriptional Tat circuit (Razooky and Weinberger, 2011). The parameter k_v is the maximal V production rate, and the parameter k_M is a half-saturation constant. The parameter k_{VC}represents the negative interaction of C with V. To represent this interaction, we introduce the term Interspecific Interference Competition (IIC). IIC is represented by the multiplication of the concentration of the interacting species and an interference coefficient (Hsu, 1981). IIC was chosen to represent this negative interaction because of its simplicity and low non-linearity. The parameter k_{dV} denotes a first-order decay rate of V (Tan et al., 2012). The parameter k_C denotes the basal production rate of C. The second term represents the negative interaction of V with C, which was generated following the same logic of considering the negative interactions in the form of an IIC. The parameter k_{dC} represents the first-order decay of C (Tan et al., 2012). All the parameters in the equations have positive ranges defined by experimental reports and are tabulated in Table 1. We proposed nominal values within the defined ranges.

3.1. Initial conditions

We proposed four initial conditions that describe the relevant biological situations. In case 1, we represented a cell with an integrated HIV provirus but null expression of HIV proteins and no CRFs ($V(0)=0$, $C(0)=0$). In case 2, following (Huang et al., 2007; Wu, 2012), who experimentally generated constitutive CRF expression, we propose a system that starts at ($V(0)=0$, $C(0)=1000$). Case 3 represents the preintegration transcription of the HIV provirus (Wu, 2004). Here, a low initial number of HIV proteins and no CRF was assumed ($V(0)=5$, $C(0)=0$). In case 4, we proposed combining the previous two scenarios to represent a system that begins with a low count of HIV proteins and prior expression of CRFs ($V(0)=5$, $C(0)=1000$).

3.2. Defining latent and productive states

The latent and productive HIV phenotypes are defined by the gene expression of HIV. In the simulations, we used the dynamics of V to define a threshold to differentiate latent and productive states. The latent HIV phenotype is characterized by null expression of viral gene products (Donahue and Wainberg, 2013). In our simulations, a null concentration of V (i.e., $V<1$ molecule/cell) defined the system as being in the virus non-productive (VNP) state. In contrast, the productive HIV phenotype is characterized by active expression of viral gene products. Previous studies that considered the intracellular dynamics of HIV have determined values for the steady state concentrations of the full HIV mRNA that vary from 1000 to 6000 molecules/cell (Kim and Yin, 2005). In our simulations we assumed the virus-productive (VP) state if V reached values inside the orders of magnitude of the steady states of the full HIV mRNA (i.e., $V\in[1000, 10{,}000]$ molecules/cell).

3.3. Deterministic dynamic behavior of the system

To determine the steady states in the system, we assumed a quasi-steady-state in Eq. (2). After solving for C and substituting into Eq. (1), the system was reduced to

$$\dot{V} = k_V/100 + k_V(V/(V+k_M)) - k_{VC}V(k_C/(k_{dC}+k_{CV}V)) - k_{dV}V. \quad (3)$$

Then, setting Eq. (3) equal to zero, we obtained an algebraic equation whose roots indicate no change in the system's dynamics and hence the presence of steady states. Symbolic methods from Mathematica™ were used to obtain analytical expressions of those roots. Additionally, deterministic simulations were used to determine the time evolution of the system. With this strategy, we corroborated whether the system under different initial conditions evolved into two different stable steady states.

3.4. Stochastic dynamic behavior of the system

Initially, after viral infection, very low amounts of HIV proteins are present in an HIV-infected cell. Low molecular counts of HIV proteins exhibit large fluctuations in reaction processes (Weinberger et al., 2005). To determine the stochastic effects of the switching behavior of the model, we applied stochastic analysis by two approaches. The first one is an approximation that uses transition state theory to determine the influence of the biochemical noise in the VNP--VP switching decision (Kramers, 1940). The second one uses the direct method of the stochastic simulation algorithm (SSA) to directly track the effects of intrinsic noise in trajectories that represent individual HIV-infected cells (Gillespie, 1976).

3.4.1. Transition state theory

To determine the influence of the biochemical noise in the VNP--VP switching decision, we considered a stable distribution of cell states in the presence of random fluctuations. This idea is reminiscent of statistical physics, where randomness results from

Table 1
Parameter definitions and range values.

Parameter	Description	Nominal value	Range	Units	Refs.
[a]k_{BV}	Basal expression rate of V	1.34×10^{-3}	$[0, 1\times10^{-2}]$	Molecules/s	Nabel and Baltimore (1987)
k_M	Michaelis-constant	380	$[1\times10^{2}, 1\times10^{4}]$	Molecules	Slice et al. (1992)
k_V	Maximal expression rate of V	1.34×10^{-1}	[0, 1]	Molecules/s	Reddy and Jhon (1999)
[b]k_C	Expression rate of C	7×10^{-2}	$[0, 1\times10^{-1}]$	Molecules/s	Schwanhäusser et al. (2011)
k_{VC}	Interference coefficient from C against V	2.95×10^{-2}	[0, 1]	1/Molecules*s	This study
k_{CV}	Interference coefficient from V against C	9.27×10^{-1}	[0, 1]	1/Molecules*s	This study
k_{dV}	Decay rate of V	6.85×10^{-5}	$[0, 1\times10^{-4}]$	1/s	Reddy and Jhon (1999)
k_{dC}	Decay rate of C	5.01×10^{-5}	$[0, 1\times10^{-4}]$	1/s	Phillips et al. (2010)

[a] Parameter k_{BV} was redefined as $k_{BV}=k_V/100$. According to (Nabel and Baltimore, 1987).
[b] Parameter k_C contains IFN effects, $k_C=k_C'$[IFN], where k_C' and [IFN] are constants.

thermal fluctuations and the stable distribution of states reflects a potential energy function (Sisan et al., 2012).

Following (Strogatz, 1994), we redefine the right hand side of Eq. (3) as the potential-like function

$$U_V = -\int F(V)dV, \tag{4}$$

and, after integrating Eq. (4), a potential-like landscape emerges. In a potential-like landscape, the local minima correspond to stable cell states. Notice that in our system the stable cell states correspond to the VNP and VP states. In a landscape composed of multiple minima, transitions from one stable state to another are possible if there is a force that drives those fluctuations. In Eq. (4) we assumed that this force is introduced by a Gaussian white noise source (β). Therefore, we obtained the following Langevin equation:

$$\dot{V} = (k_V/100 + k_V(V/(V+k_M)) - k_{VC}V(k_C/(k_{dC}+k_{CV}V)) - k_{dV}V) + \beta, \tag{5}$$

where the lower bound of the intensity of β is the coefficient of variation (η) defined as

$$\eta = 1/\sqrt{N}, \tag{6}$$

where N is the molecular count of V (Nguyen and Kulasiri, 2011).

Using Eq. (5), we made use of the standard transition-rate theory that states the escape rate is proportional to the exponential of the negative of the energy-barrier height (ΔU) separating this basin from the surrounding state, divided by the intensity of β. Therefore, the probability per unit time that the molecule state leaves the basin is proportional to the following expression: $\exp(-\Delta U/\eta)$ (Kramers, 1940).

According to the previous discussion, the cell escape rates from one local minimum to another are defined from the basin VNP into VP ($p_{\text{VNP-VP}}$) and from the basin VP into VNP ($p_{\text{VP-VNP}}$), Eqs. (7) and (8), respectively.

$$p_{\text{VNP}-\text{VP}} = Ae^{-k\frac{\Delta U_{\text{VNP}}}{\eta}}, \tag{7}$$

$$p_{\text{VP}-\text{VNP}} = Ae^{-k\frac{\Delta U_{\text{VP}}}{\eta}}, \tag{8}$$

where k and A are proportionality constants.

To extend our analysis from a single cell to study the dynamics of cell populations, we defined the cellular flux that determines the number of cells that escape from the basin VNP into VP ($J_{\text{VNP-VP}}$) and vice versa ($J_{\text{VP-VNP}}$) as follows:

$$J_{\text{VNP}-\text{VP}} = N_{\text{VNP}}(p_{\text{VNP}-\text{VP}}), \tag{9}$$

$$J_{\text{VP}-\text{VNP}} = N_{\text{VP}}(p_{\text{VP}-\text{VNP}}), \tag{10}$$

N_{VNP} and N_{VP} are the number of cells whose states are trapped in the basins VNP and VP, respectively.

In the dynamic equilibrium, the cellular fluxes from the basin VNP into VP are equal

$$N_{s\text{VNP}}(p_{\text{VNP}-\text{VP}}) = N_{s\text{VP}}(p_{\text{VP}-\text{VNP}}), \tag{11}$$

where $N_{s\text{VNP}}$ and $N_{s\text{VP}}$ denote the equilibrium cell counts in the states VNP and VP, respectively.

Substituting the escape rates, the ratio of cells in the VNP and VP state was expressed as follows:

$$\frac{N_{s\text{VNP}}}{N_{s\text{VP}}} = \frac{p_{\text{VP}-\text{VNP}}}{p_{\text{VNP}-\text{VP}}} = \frac{e^{-k(\Delta U_{\text{VP}}/\eta)}}{e^{-k(\Delta U_{\text{VNP}}/\eta)}} \tag{12}$$

Finally, the empirical probability of obtaining cells in the VNP state was defined as

$$P(\text{VNP}) = N_{s\text{VNP}}/(N_{s\text{VNP}} + N_{s\text{VP}}), \tag{13}$$

and the empirical probability of obtaining cells in the VP state was defined as

$$P(\text{VP}) = 1 - P(\text{VNP}). \tag{14}$$

3.4.2. Stochastic simulations

Stochastic simulations were used to determine the transitions from the VNP to the VP states in individual trajectories that represent unique HIV-infected cells. Here, we converted the system given by Eqs. (1) and (2) into a reaction rate scheme (Table 3). To obtain this reaction scheme, we used the terms of production and degradation in our system equations as elementary complex reactions that can be represented by a single step (Keizer, 1987). We then implemented the direct method of the SSA for 1000 realizations under a short simulated time (50 h) and for a long simulated time (21 days). At the end of the simulated time, the dispersion of trajectories was used to construct cell distribution histograms. Analysis of the distribution histograms allowed us to determine the bimodal dynamics.

3.5. Exploring the parameter space

To determine the generality of our model results, we performed a massive exploration in the parameter space. Here we defined parameter values that vary in orders of magnitude (see Table 1). We then implemented Monte-Carlo scanning (Metropolis and Ulam, 1949) to generate 10,000 pseudorandom parameter sets in three independent repetitions. Each parameter set was iteratively tested on the previously described deterministic and stochastic analyses.

To represent our results, we redefined the parameters and variables for the model given by Eq. (3) as described in Table 2 to obtain the dimensionless model

$$\dot{v} = a_v/100 + a_v(v/(v+1)) - (p_{vc}v/(1+p_{cv}v)) - v. \tag{15}$$

Parameters p_{vc} and p_{cv} were chosen to build a two-dimensionless parameter space. Notice that parameters $p_{vc} \propto k_{VC}$ *and* $p_{cv} \propto k_{CV}$ (for an exact definition, see Table 2); therefore, they represent the strength of the negative interactions between V and C.

With this equation, we represent (1) the parameter space that reproduces bistable behavior, (2) the effects of the biochemical noise in the VNP–-VP decision along the parameter space, and (3) the parameter space where stochastic simulations can reproduce bimodal behavior.

3.6. Numerical methods

The Monte-Carlo-type scanning, the numerical integration of the potential-like functions, the estimation of the empirical probability of obtaining cells in the VP and VNP states and the SSA were carried out with MATLAB (v7. The MathWorks Inc., Natick, MA).

Table 2
Parameters and variables in the dimensionless model.

Parameter/variable	Definition
a_v	$k_V/(k_{dv} \times k_M)$
p_{vc}	$k_C\ k_{VC}/(k_{dV} \times k_{dC})$
p_{cv}	$k_M\ k_{CV}/k_{dC}$
v	V/k_M
τ	$k_{dV}t$

Table 3
Reaction scheme for the model given in Eqs. (1) and (2).

Reactions	Description	Effective propensity
$\varnothing \rightarrow V$	Basal production of V	k_{BV}
$\varnothing \rightarrow V$	Production of V enhanced by transactivation	$k_V\,(V/(V+k_M))$
$V \rightarrow \varnothing$	Interference competition between C and V	$k_{VC}VC$
$V \rightarrow \varnothing$	Decay of V	$k_{dV}V$
$\varnothing \rightarrow C$	Constant production of C	k_C
$C \rightarrow \varnothing$	Interference competition between V and C	$k_{CV}VC$
$C \rightarrow \varnothing$	Decay of C	$k_{dC}C$

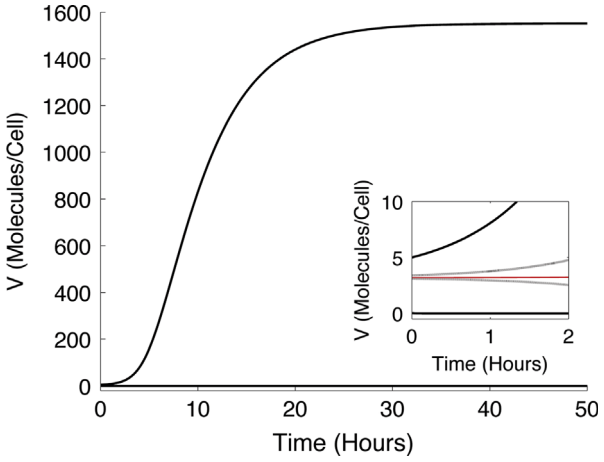

Fig. 2. Deterministic simulations using two different initial conditions ($V(0)=0$, $C(0)=0$ and $V(0)=5$, $C(0)=0$) give rise to two stable states (black solid lines). An unstable steady state is reached using the initial conditions $V(0)=3.19$, $C(0)=0.02$ (red line). Using two different sets of initial conditions ($V(0)=3.1$, $C(0)=0.02$ and $V(0)=3.4$, $C(0)=0.02$) close to the previous unstable steady state, we obtain stability (gray lines). Inset zooms out the y-axis. The representative example was made with the nominal parameter values given in Table 1. (For interpretation of the references to color in this figure legend, the reader is referred to the web version of this article.)

4. Results

4.1. Deterministic dynamic behavior of the system

We first studied the multiple steady states in the HIV molecular interaction network given by Eqs. (1) and (2). We set the right-hand side in Eq. (2) equivalent to zero. We solved for C and substituted the result into Eq. (1). We found three roots for V^*. Substituting these V^* values in Eq. (2) and solving for C, we obtained the corresponding values for C^*. All the parameters kept the nominal values in Table 1. We obtained the following three steady states of the system (ss): ss1 ($V^*=8\times10^{-5}$, $C^*=559$), ss2 ($V^*=3.19$, $C^*=2\times10^{-2}$) and ss3 ($V^*=1551$, $C^*=4.8\times10^{-5}$). Furthermore, we numerically solved the model equations taking into account all the initial conditions previously described (see Section 3.1.). We corroborated that the system evolved to two different stable steady states that correspond to ss_1 and ss_3 (see Fig. 2, black solid lines). Then, using the values obtained for ss_2 and two additional values close to this point as the initial conditions, we determined that this steady state is unstable (see Fig. 2, red line and gray lines).

To understand the effect that the terms of the interspecific interference competition have in the model, we determined the negative influence between V and C in the system dynamics. To do this, we numerically solved the complete system (Eqs. (1) and (2)) using nominal parameter values and assuming k_{VC} and k_{CV} as free parameters. We obtained a bifurcation diagram that contains three

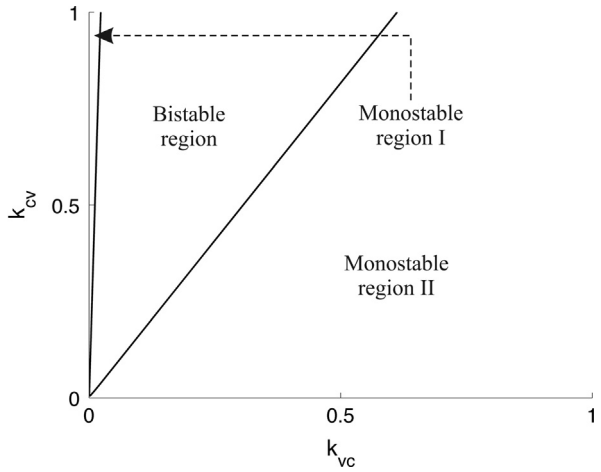

Fig. 3. Two-dimensional bifurcation diagram. Simulations were made with the nominal values given in Table 2 and varying the undetermined parameters k_{CV} and k_{VC} in the range [0, 1]. Low values for k_{VC} reproduce a narrow monostable area. Intermediate values of k_{VC} reproduce a bistable region. Large values of k_{VC} reproduce a monostable area.

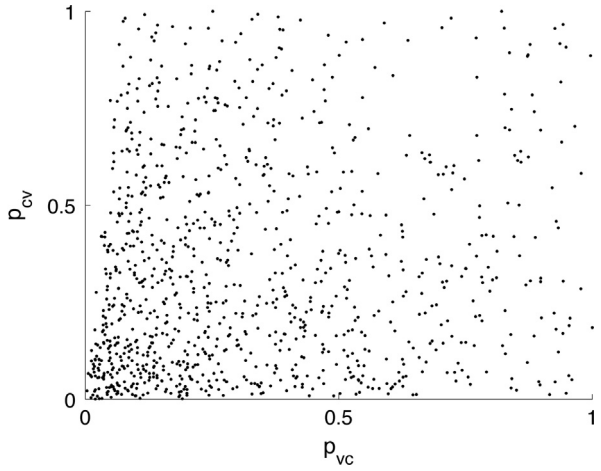

Fig. 4. Parameter space that reproduces bistable dynamics. Black dots represent bistable cases. The parameters p_{vc} and p_{cv} correspond to the x- and y-axis, respectively. Every axis is normalized, and extreme values were eliminated.

different dynamic regions (see Fig. 3). The first region is a narrow monostable region that was obtained when low values for the parameter k_{VC} were given. A second region was obtained when intermediate values of k_{VC} were given that reproduces bistable behavior. A third region was obtained when high values of k_{VC} were given that reproduces monostable behavior. In this bifurcation diagram, bistable behavior was obtained in a wide area but it was biased toward low values of the parameter k_{VC}.

We then examined whether bistability is maintained over a wide range of parameter values. After testing 10,000 pseudorandom parameters that vary in the ranges defined in Table 1, we found that approximately 12% of those parameters reproduce bistable dynamics. A complete distribution of those parameters in the parameter space did not reflect a restriction in their values. The results are shown in Fig. 4.

We further analyzed the distribution of steady states in parameter sets that reproduce bistable dynamics. In Fig. 5, we plot every bistable case along the x-axis and the value for V that corresponds to every steady state in the y-axis. As expected, we found two stable steady states and one unstable steady state for each bistable case. For all cases, the first stable steady state was found at $V\approx0$ (Fig. 5, black dots at the bottom). Most unstable

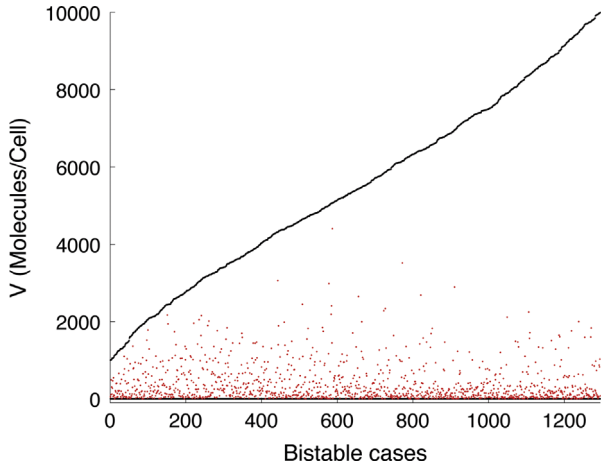

Fig. 5. Distribution of steady states in each bistable case. In the left graph, every x point represents a bistable case and has three vertical points that correspond to its three steady states. Red dots represent unstable steady states, while black dots represent stable steady states. Bistable cases were ordered by the V value in the third steady state. (For interpretation of the references to color in this figure legend, the reader is referred to the web version of this article.)

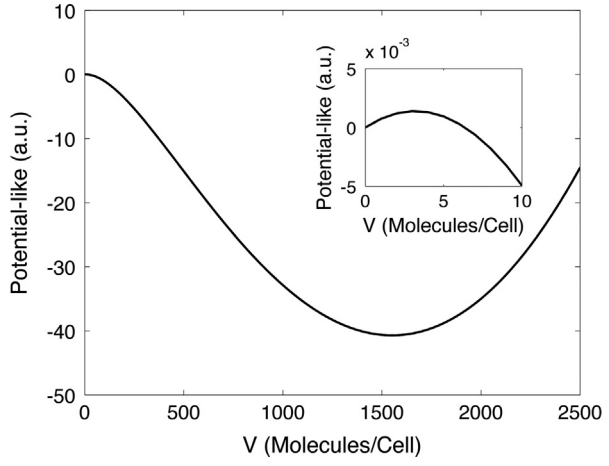

Fig. 6. Potential-like landscape. Local minima correspond to stable steady states. Local maxima correspond to unstable steady states. Inset zooms on the x-axis and shows the local maxima. The representative example was made with the nominal parameter values given in Table 1. (For interpretation of the references to color in this figure legend, the reader is referred to the web version of this article.)

steady states were found distributed in the range $V \approx (0,\ 2000)$ (Fig. 5, red dots), and the second stable steady state was found distributed over $V > 1000$ (Fig. 5, upper black dots).

4.2. Stochastic dynamic behavior of the system

4.2.1. Transition-state theory

After determining that our system reproduces bistable dynamics, we extended our analyses to study how the intensity of biochemical noise affects the VNP--VP switching decision. Using nominal values for the parameters and numerically integrating Eq. (4), we obtained a potential-like landscape with two local minima that correspond to the VNP and VP states, respectively (see Fig. 6). We observed an asymmetric potential representative of all parameter sets that present bistability.

Using our potential landscape, we applied transition-state theory using a fixed value of intensity for the biochemical noise ($\eta = 0.0032$, $N = 100{,}000$) and found that the system has a high probability of reaching the VP state once in equilibrium ($P(\mathrm{VP}) \approx 1$). We applied transition-state theory to all positive bistable cases generated after the

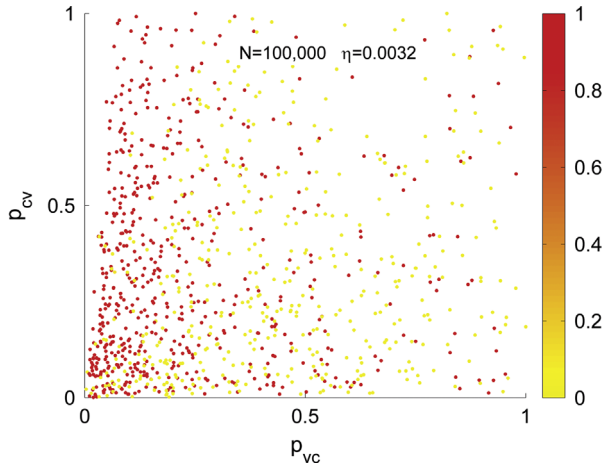

Fig. 7. The empirical probability of obtaining cells in the VP state according to the parameter values. Simulation results using a molecular count $N = 100{,}000$ and $\eta = 0.003$. In the scatter plot, each point represents a set of parameters that resulted in a system with bistable behavior. The point color represents the empirical probability of obtaining cells in the VP state. (For interpretation of the references to color in this figure legend, the reader is referred to the web version of this article.)

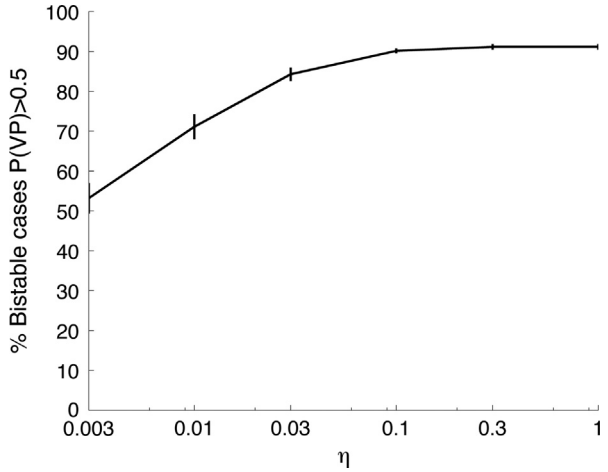

Fig. 8. Percentage of total bistable cases with an empirical probability of obtaining cells in the VP state higher than 0.5 ($P(\mathrm{VP}) > 0.5$) under different intensities of η. We calculated the error bars from three repeats of numerical experiments.

Monte-Carlo scanning. In the first instance we solved our equations using $\eta = 0.0032$. The scatter plot in Fig. 7 shows the empirical probability of obtaining the VP state as the colored points. As the inhibition from CRF towards HIV proteins becomes less effective (low nominal value in p_{VC}), the VP state becomes more probable (red dots).

We explored how different intensities of biochemical noise modify the VNP--VP switching decision. To do this, we used transition-state theory again but now in the range $\eta = [0.0032,\ 1]$. Fig. 8 shows the percentage of bistable cases that showed a probability of obtaining cells in the VP state higher than 0.5. This threshold indicates when it is more probable to obtain cells in the VP than in the VNP state. Our results showed that as we increased η, the percentage of bistable cases with a high probability of obtaining the VP state increases. In contrast, if η is decreased to values near zero, we approach a purely deterministic regime where no decision is expected.

4.2.2. Stochastic simulations

To directly track the effects of biochemical noise in trajectories that represent individual HIV-infected cells, we carried out stochastic simulations. The SSA was implemented (see Section

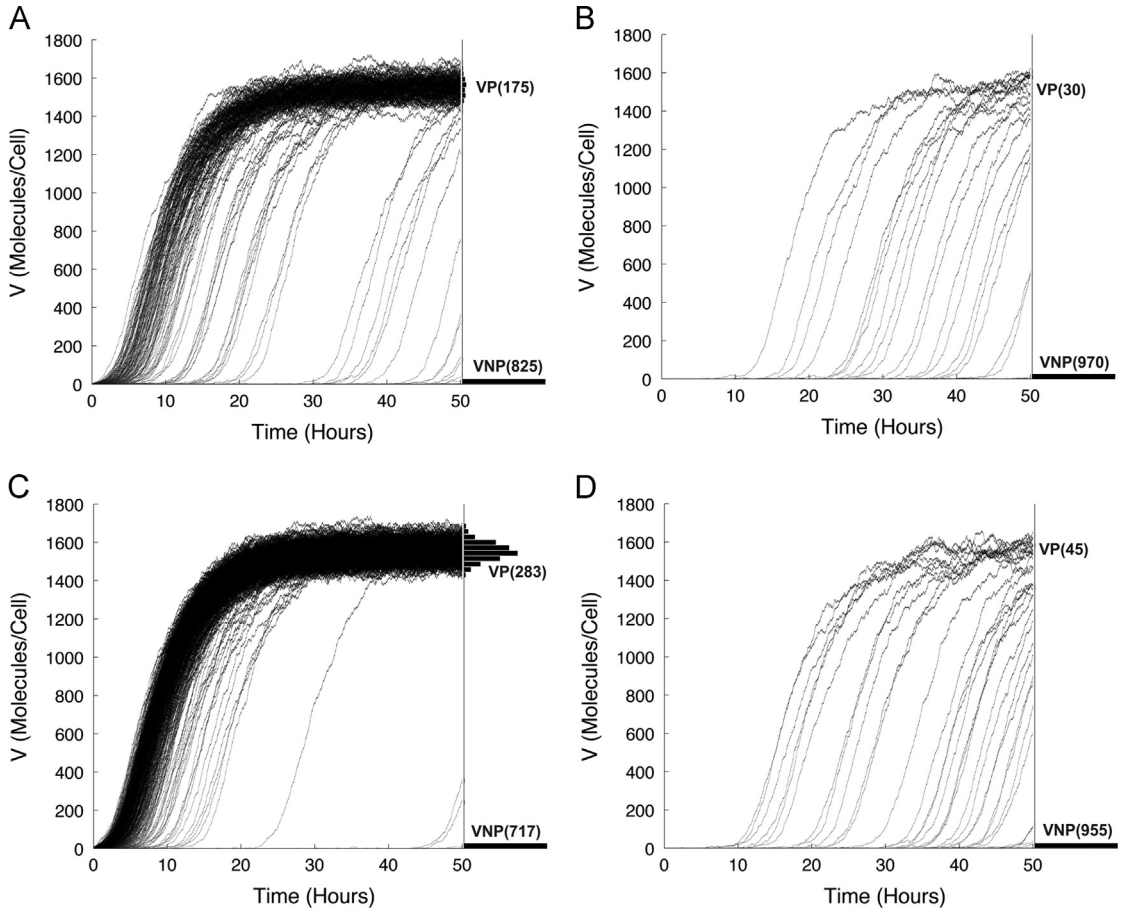

Fig. 9. Stochastic simulation results for 1000 individual trajectories that represent single-cell dynamics are shown for a simulated timespan of 50 h. On the right, a histogram of the final trajectories is given. VNP and VP legends are used to indicate those states. (A) Using the initial conditions $V(0)=0$, $C(0)=0$. (B) Using the initial conditions $V(0)=0$, $C(0)=1000$. (C) Using the initial conditions $V(0)=5$, $C(0)=0$. (D) Using the initial conditions $V(0)=5$, $C(0)=1000$. The representative example was made with the nominal parameter values given in Table 1.

3.2.). A first set of 1000 trajectories was made using the nominal parameter values given in Table 1 and a simulated timespan of 50 h. Using the initial condition ($V(0)=0$, $C(0)=0$), a bimodal distribution where the VNP state was more common and a small fraction of trajectories ended in the VP state was obtained (Fig. 9A). For the second initial condition ($V(0)=0$, $C(0)=1000$), we found that CRFs interfered with the transition to the VP state, and most trajectories ended in the VNP state (Fig. 9B). In the third initial condition ($V(0)=5$, $C(0)=0$), we found that an initial count of five HIV proteins produced a substantial increase in the number of trajectories that end in the VP state (Fig. 9C). In the fourth initial condition ($V(0)=5$, $C(0)=1000$), we found that even with a low count of HIV proteins the transition to the VP state was inhibited if CRFs were already expressed (Fig. 9D).

To determine the temporary stability of the obtained stochastic dynamics, we carried out the SSA for large periods of time (21 days of simulated time) and obtained similar dynamics to those obtained over 50 h. However, for the longer simulations, the stochastic transitions from trajectories in the VNP to the VP state were more evident (see Fig. 10A–D).

Finally, to determine the parameter space that reproduces bimodal dynamics, we implemented the SSA for all parameters generated by the Monte-Carlo scanning. Histograms for the trajectories at the end of the simulated time were obtained. In those histograms, we determined whether bimodal distributions were present. In Fig. 11, we present the parameter space that reproduces bimodal dynamics. It should be noted that the region that reproduces bimodal dynamics is obtained with low nominal values of the parameter p_{vc}.

5. Discussion

Understanding the intracellular dynamics of HIV by considering the mechanisms of HIV gene expression and the innate immune response is essential for predicting the manifestation and outcome of HIV infection.

In this paper, we proposed a mathematical model that is made up of two main elements; the first one is a positive feedback loop that represents HIV gene expression enhanced by the transcriptional Tat-circuit. The second element represents the mutual negative interaction between the innate immune response and HIV proteins. Previous studies have considered the mutual negative interaction between the innate immune system and viral proteins but have not considered the positive feedback loop in HIV production (Tan et al., 2012; Zou et al., 2010). Other previous studies have considered the positive feedback loop in virus production but have not considered the mutual negative interaction between the innate immune system and HIV proteins (Konkoli and Jesorka, 2013; Razooky and Weinberger, 2011; Weinberger and Shenk, 2007; Weinberger et al., 2005). We propose a simple model that takes both interactions described above into account.

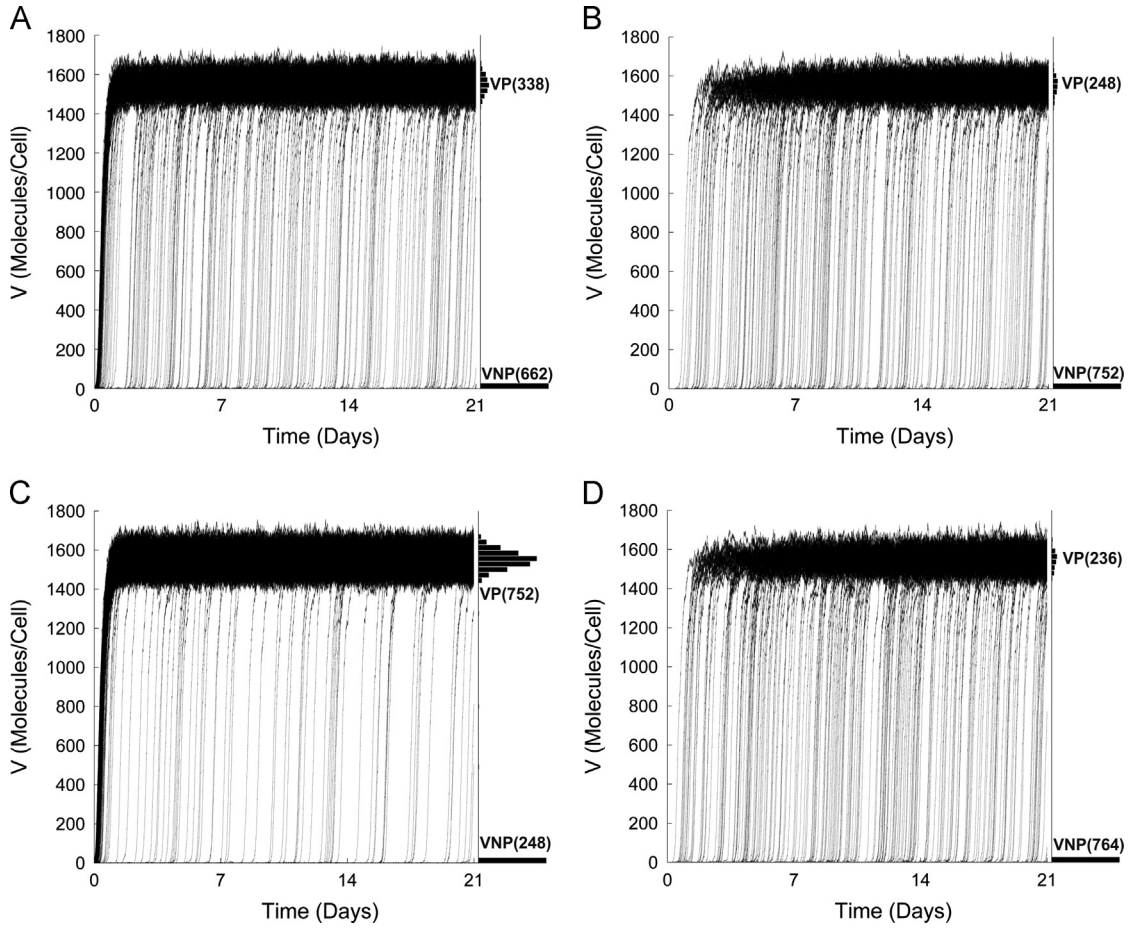

Fig. 10. Stochastic simulation results for 1000 individual trajectories that represent single-cell dynamics are shown for a simulated timespan of 21 days. On the right, a histogram of the final trajectories is given with the number of cells that end in each distribution. VNP and VP legends are used to indicate those states. A) Using the initial conditions $V(0)=0$, $C(0)=0$. B) Using the initial conditions $V(0)=0$, $C(0)=1000$. C) Using the initial conditions $V(0)=5$, $C(0)=0$. D) Using the initial conditions $V(0)=5$, $C(0)=1000$. The representative example was made with the nominal parameter values given in Table 1.

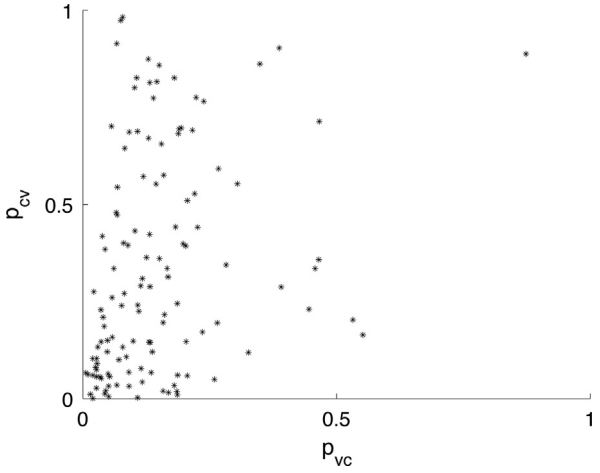

Fig. 11. Parameter space that reproduces bimodal dynamics using the initial conditions $V(0)=0$, $C(0)=0$. Black dots represent bimodal cases. The parameters p_{vc} and p_{cv} correspond to the x- and y-axis, respectively. Every axis is normalized, and extreme values were eliminated. Simulations made using different initial conditions generated similar results (data not shown). (For interpretation of the references to color in this figure legend, the reader is referred to the web version of this article.)

5.1. Deterministic dynamic behavior of the system

Our mathematical model reproduced bistable dynamic behavior (see Fig. 2). Self-cooperativity in positive-feedback loops can generate multistability and provides a mechanism for choosing between alternate fates. Nevertheless, previous studies have discarded the possibility of self-cooperativity in a Tat positive-feedback loop (Weinberger and Shenk, 2007). Additionally, previous studies have represented innate immune responses by Hill-type functions and obtained viral intracellular dynamics that include monostability, bistability and oscillations (Tan et al., 2012; Zou et al., 2010). In our model, bistability was obtained in a different way. Bistability is the result of the combined effect of a double negative interaction and a positive feedback loop with low non-linearity (*i.e.* no Hill-type functions). Monostable dynamics were obtained if negative interactions or the positive feedback loop were considered separately (data not shown).

The strength of the mutual negative interaction between the innate immune response and HIV proteins was determined in a bifurcation diagram. A bistable region was obtained as the result of the strength of those interactions (see Fig. 3). Additionally, we determined that multiple parameter combinations reproduce bistable dynamics (see Fig. 4). These results indicated that the model was able to reproduce bimodal dynamics in wide ranges of parameter values.

The distribution of steady states in multiple bistable cases was determined according to the value of V. We obtained one stable steady state at $V \approx 0$ and another stable steady state at $V > 1000$ for all cases (see Fig. 5). Those steady states represent the VNP and VP cell states. Considering the given initial conditions (Section 3.1.), only two possible outputs were obtained; the first one was a system that began in the VNP and stayed there, and the other one

was a system that started near the VNP state and evolved to the VP state. Stochasticity was needed to explain transitions between states.

5.2. Stochastic dynamic behavior of the system

HIV intracellular dynamics are strongly affected by the effects of biochemical noise (Balázsi et al., 2011). To determine the effect of biochemical noise in the network, we analyzed stochasticity by transition-state theory and by the direct method of the SSA.

5.2.1. Transition-state theory

Using transition-state theory, we determined that the effects of biochemical noise vary across the parameter space. The VP state was favored when low nominal values of p_{vc} were given (see Fig. 7, red dots). Then, we determined that, as the intensity in the biochemical noise increased, there was an increase in the probability of obtaining the VP state (see Fig. 8). Our results agree with previous studies that proved that biochemical noise is detrimental to the latency decision (Konkoli and Jesorka, 2013; Razooky and Weinberger, 2011; Weinberger and Shenk, 2007; Weinberger et al., 2008, 2005).

5.2.2. Stochastic simulations

Stochastic simulations reproduced temporal bimodal dynamics with transitions from the VNP to the VP state (see Fig. 9). Comparing our results with the stochastic dynamics of the transcriptional Tat circuit, significant differences were identified. The stochastic dynamics of the Tat circuit reproduces non-bistable temporary bimodal dynamics were cells in the VP state eventually return to the VNP state (Razooky and Weinberger, 2011; Weinberger et al., 2005).

The conditions of the cell before infection may contribute to the entry into the latent or productive phenotype. An initial molecular count of HIV proteins above zero at the beginning of stochastic simulation reduces the probability of obtaining cells in the latent state and enhances the stochastic transitions to the VP state (see Fig. 9B and D). Previous reports considered an initial count of HIV proteins above zero to be required to obtain bimodal behavior (Althaus and De Boer, 2010; Weinberger et al., 2005). However, if CRFs are already expressed in the system, the probability of obtaining a latent state increases (see Fig. 9B and D). This results is corroborated by previous experimental studies in which the expression of CRF in infected cells increased the probability that those cells exhibited the latent phenotype (Huang et al., 2007; Wu, 2012).

Stochastic dynamics for long periods of time (21 days) showed accumulative transitions from the VNP to the VP state (see Fig. 10A–D). Nevertheless, it was not possible to detect transitions from the VP to the VNP state. For this reason, it is expected that simulations could only achieve monomodal behavior. This predicted temporal bimodal behavior may explain the dynamics obtained for long-term infection under HAART characterized by a decline in HIV concentration and intermittent viral blips (Rong and Perelson, 2009).

Comparing the results obtained by transition-state theory and SSA, we determined that the strength of the interactions between innate immune response and HIV proteins affects the final VNP or VP state. Specifically, we found that low nominal values of p_{vc} and high nominal values of the parameter p_{cv} favor the VP state (Fig. 7, red dots and Fig. 11, black dots). The genetic background of each individual could determine p_{vc}. Polymorphisms in genes with innate antiviral function, for example CRF, may affect gene expression and protein function, thus contributing to HIV susceptibility and disease progression (Barr, 2010). However, the parameter p_{cv} could be determined by the specific anti-restriction mechanism of the HIV protein, which could also be affected by the genetic background of the given viral strain (Eriksson et al., 2013).

5.2.3. Biological implications

To reproduce bistable and bimodal dynamics, we find that at least two conditions must be fulfilled in the biological system. The first one is the expression and functionality of the CRF, and the second one is the presence of a viral mechanism that counteracts the activity of the CRF. Both conditions guarantee a mutual double-negative interaction and the non-linearity needed in the mathematical model to obtain bistable and bimodal dynamics.

Referring to the first condition, few CRFs are determined to be overexpressed and functional in resting memory T4 cells (Baldauf et al., 2012; Ganesh et al., 2003; Huang et al., 2007). Some CRFs have been described in active T4 cells, which could indicate their presence in resting memory T4 cells, but this is still speculative. Nevertheless, the presence of many more currently undiscovered CRFs in different cell lines is a real possibility (Blanco-Melo et al., 2012; Tyagi and Kashanchi, 2012). For example, in a whole genome screen, 114 unknown CRFs with significant inhibition of HIV infection were identified in Hela-CD4+ cells (Liu et al., 2011). In addition, we noticed in our literature search that many studied CRFs are involved in preintegration steps in the virus replication cycle (i.e., APOBEC3G (Zhang et al., 2003) and SAMHD1 (Lahouassa et al., 2012)). Those CRFs were not considered in this study because their effect cannot account for the long-term latency observed during HAART.

Referring to the second condition, we found that most viral mechanisms that counteract the activity of CRF are not fully defined. It is theoretically possible that a recently evolved restriction factor might not yet have been selected for a viral antagonist. However, in most cases, the inability to identify a viral antagonist is more likely to be attributable to the lack of information about the versatile functions of the HIV proteins (Zack et al., 2013). Finally, if no viral counter-mechanism is present, a scenario in which CRF limits the VP state could be obtained, something already proven in cell lines coexpressing the transcriptional Tat circuit and the human protein Srt1 (Weinberger et al., 2008).

6. Conclusion

In this study, we combined deterministic and stochastic approaches to analyze the behavior of HIV proteins and the innate immune response. Using wide ranges of parameter values, our results predicted the following: (1) a phenomenological description of the viral productive and latent cell phenotypes is obtained by bistable and temporal bimodal dynamics, (2) biochemical noise reduces the probability that an infected cell adopts the latent state, (3) the effects of the innate immune response enhances the HIV latency state, (4) the conditions of the cell before infection affects the acquisition of the latent phenotype, i.e., the existing expression of cell restriction factors propitiates HIV latency and, in contrast, existing HIV proteins reduce HIV latency.

Acknowledgements

This research was partially supported by Consejo Nacional de Ciencia y Tecnología (CONACYT, MEXICO) under grant 105649.

References

Abbas, W., Herbein, G., 2012. Molecular understanding of HIV-1 latency. Adv. Virol 2012, 1–14, http://dx.doi.org/10.1155/2012/574967.

Adrews, S.S., Dinh, T., Arkin, A.P., 2009. Stochastic models of biological processes. Encycl. Complexity Syst. Sci, 8730–8749.

Althaus, C.L., De Boer, R.J., 2010. Intracellular transactivation of HIV can account for the decelerating decay of virus load during drug therapy. Mol. Syst. Biol. 6, 348, http://dx.doi.org/10.1038/msb.2010.4.

Balázsi, G., van Oudenaarden, A., Collins, J.J., 2011. Cellular decision making and biological noise: from microbes to mammals. Cell 144, 910–925, http://dx.doi.org/10.1016/j.cell.2011.01.030.

Baldauf, H.M., Pan, X., Erikson, E., Schmidt, S., Daddacha, W., Burggraf, M., Schenkova, K., Ambiel, I., Wabnitz, G., Gramberg, T., Panitz, S., Flory, E., Landau, N.R., Sertel, S., Rutsch, F., Lasitschka, F., Kim, B., König, R., Fackler, O.T., Keppler, O.T., 2012. SAMHD1 restricts HIV-1 infection in resting CD4(+) T cellsNat. Med 18, 1682–1687, http://dx.doi.org/10.1038/nm.2964.

Barr, S.D., 2010. Cellular HIV-1 restriction factors: a new avenue for AIDS therapy? Future Virol 5, 417–433.

Barr, S.D., Smiley, J.R., Bushman, F.D., 2008. The interferon response inhibits HIV particle production by induction of TRIM22. PLoS Pathog. 4, e1000007, http://dx.doi.org/10.1371/journal.ppat.1000007.

Blanco-Melo, D., Venkatesh, S., Bieniasz, P.D., 2012. Intrinsic cellular defenses against human immunodeficiency viruses. Immunity 37, 399–411, http://dx.doi.org/10.1016/j.immuni.2012.08.013.

Chun, T.-W., Carruth, L., Finzi, D., Shen, X., DiGiuseppe, J.A., Taylor, H., Hermankova, M., Chadwick, K., Margolick, J., Quinn, T.C., Kuo, Y.-H., Brookmeyer, R., Zeiger, M.A., Barditch-Crovo, P., Siliciano, R.F., 1997. Quantification of latent tissue reservoirs and total body viral load in HIV-1 infection. Nature 387, 183–188, http://dx.doi.org/10.1038/246170a0.

Cojo, M.S., Lopez-Huertas, M.R., Mateos, E., Alcami, J., Coiras, M., 2011. Mechanisms of RNA interference in the HIV-1-Host cell interplay. AIDS Rev. 13, 149–160.

Donahue, D.A., Kuhl, B.D., Sloan, R.D., Wainberg, M.A., 2012. The viral protein Tat can inhibit the establishment of HIV-1 latency. J. Virol. 86, 3253–3263, http://dx.doi.org/10.1128/JVI.06648-11.

Donahue, D.A., Wainberg, M.A., 2013. Cellular and molecular mechanisms involved in the establishment of HIV-1 latency. Retrovirology 10, 11, http://dx.doi.org/10.1186/1742-4690-10-11.

Duggal, N.K., Emerman, M., 2012. Evolutionary conflicts between viruses and restriction factors shape immunity. Nat. Rev. Immunol. 12, 687–695, http://dx.doi.org/10.1038/nri3295.

Eriksson, S., Graf, E.H., Dahl, V., Strain, M.C., Yukl, S.A., Lysenko, E.S., Bosch, R.J., Lai, J., Chioma, S., Emad, F., Abdel-Mohsen, M., Hoh, R., Hecht, F., Hunt, P., Somsouk, M., Wong, J., Johnston, R., Siliciano, R.F., Richman, D.D., O'Doherty, U., Palmer, S., Deeks, S.G., Siliciano, J.D., 2013. Comparative analysis of measures of viral reservoirs in HIV-1 eradication studies. PLoS Pathog. 9, e1003174, http://dx.doi.org/10.1371/journal.ppat.1003174.

Espert, L., Degols, G., Lin, Y.-L., Vincent, T., Benkirane, M., Mechti, N., 2005. Interferon-induced exonuclease ISG20 exhibits an antiviral activity against human immunodeficiency virus type 1. J. Gen. Virol. 86, 2221–2229, http://dx.doi.org/10.1099/vir.0.81074-0.

Ganesh, L., Burstein, E., Guha-niyogi, A., Louder, M., Mascola, J., Klomp, L.W., Wijmenga, C., Duckett, C., S., Nabe, l G., 2003. The gene product Murr1 restricts HIV-1 replication in resting CD4 1 lymphocytes. Nature 426, 853–857.

Gillespie, D.T., 1976. A general method for numerically simulating the stochastic time evolution of coupled chemical reactions. J. Comput. Phys. 22, 403–434, http://dx.doi.org/10.1016/0021-9991(76)90041-3.

Hsu, S., 1981. On a Resource Based Ecological Competition Model with Interference. J. Math. Biol 52, 45–52.

Huang, J., Wang, F., Argyris, E., Chen, K., Liang, Z., Tian, H., Huang, W., Squires, K., Verlinghieri, G., Zhang, H., 2007. Cellular microRNAs contribute to HIV-1 latency in resting primary CD4+ T lymphocytes. Nat. Med 13, 1241–1247, http://dx.doi.org/10.1038/nm1639.

Jordan, A., Defechereux, P., Verdin, E., 2001. The site of HIV-1 integration in the human genome determines basal transcriptional activity and response to Tat transactivation. EMBO J. 20, 1726–1738, http://dx.doi.org/10.1093/emboj/20.7.1726.

Karn, J., Stoltzfus, C.M., 2012. Transcriptional and posttranscriptional regulation of HIV-1 gene expression. Cold Spring Harb. Perspect. Med 2, a006916, http://dx.doi.org/10.1101/cshperspect.a006916.

Keizer, J., 1987. Statistical Thermodynamics of Nonequilibrium Processes, first ed. Springer.

Kim, H., Yin, J., 2005. Robust growth of human immunodeficiency virus type 1 (HIV-1). Biophys. J. 89, 2210–2221, http://dx.doi.org/10.1529/biophysj.104.058438.

Kirchhoff, F., 2010. Immune evasion and counteraction of restriction factors by HIV-1 and other primate lentiviruses. Cell Host Microbe 8, 55–67, http://dx.doi.org/10.1016/j.chom.2010.06.004.

Klipp, E., Liebermeister, W., Wierling, C., Kowald, A., Lehrach, H., Herwig, R., 2011. Systems Biology. Wiley-Blackwell.

Konkoli, Z., Jesorka, A., 2013. Fluctuations in Tat copy number when it counts the most: a possible mechanism to battle the HIV latency. Theor. Biol. Med. Model 10, 16, http://dx.doi.org/10.1186/1742-4682-10-16.

Kramers, H.A., 1940. Brownian motion in a field of force and the diffusion model. Physica, 284–304.

Lahouassa, H., Daddacha, W., Hofmann, H., Ayinde, D., Logue, E.C., Dragin, L., Bloch, N., Maudet, C., Bertrand, M., Gramberg, T., Pancino, G., Priet, S., Canard, B., Laguette, N., Benkirane, M., Transy, C., Landau, N.R., Kim, B., Margottin-Goguet, F., 2012. SAMHD1 restricts the replication of human immunodeficiency virus type 1 by depleting the intracellular pool of deoxynucleoside triphosphates. Nat. Immunol. 13, 223–228, http://dx.doi.org/10.1038/ni.2236.

Liu, L., Oliveira, N.M.M., Cheney, K.M., Pade, C., Dreja, H., Bergin, A.-M.H., Borgdorff, V., Beach, D.H., Bishop, C.L., Dittmar, M.T., McKnight, A., 2011. A whole genome screen for HIV restriction factors. Retrovirology 8, 94, http://dx.doi.org/10.1186/1742-4690-8-94.

Maitra, R.K., Silverman, R.H., 1998. Regulation of human immunodeficiency virus regulation of human immunodeficiency virus replication by 2J, 5J-oligoadenylate-dependent RNase L. J. Virol, 72.

Marcello, A., 2006. Latency: the hidden HIV-1 challenge. Retrovirology 3, 7, http://dx.doi.org/10.1186/1742-4690-3-7.

Margolis, D.M., 2010. Mechanisms of HIV latency: an emerging picture of complexity. Curr. HIV/AIDS Rep 7, 37–43, http://dx.doi.org/10.1007/s11904-009-0033-9.

Metropolis, N., Ulam, S., 1949. The Monte Carlo methodJ. Am. Stat. Assoc, 44.

Nabel, G., Baltimore, D., 1987. An inducible transcription factor activates expression of human immunodeficiency virus in T cells. Nature, 326.

Nguyen, L.K., Kulasiri, D., 2011. Distinct noise-controlling roles of multiple negative feedback mechanisms in a prokaryotic operon system. IET Syst. Biol. 5, 145–156, http://dx.doi.org/10.1049/iet-syb.2010.0020.

Okumura, A., Lu, G., Pitha-Rowe, I., Pitha, P.M., 2006. Innate antiviral response targets HIV-1 release by the induction of ubiquitin-like protein ISG15. Proc. Nat. Acad. Sci. U.S.A. 103, 1440–1445, http://dx.doi.org/10.1073/pnas.0510518103.

Palmer, S., Maldarelli, F., Wiegand, A., Bernstein, B., Hanna, G.J., Brun, S.C., Kempf, D.J., Mellors, J.W., Coffin, J.M., King, M.S., 2008. Low-level viremia persists for at least 7 years in patients on suppressive antiretroviral therapy. Proc. Nat. Acad. Sci. U.S.A. 105, 3879–3884, http://dx.doi.org/10.1073/pnas.0800050105.

Pan, X., Baldauf, H.-M., Keppler, O.T., Fackler, O.T., 2013. Restrictions to HIV-1 replication in resting CD4(+) T lymphocytes. Cell Res., 1–10, http://dx.doi.org/10.1038/cr.2013.74.

Perez-Caballero, D., Zang, T., Ebrahimi, A., McNatt, M.W., Gregory, D.A., Johnson, M.C., Bieniasz, P.D., 2009. Tetherin inhibits HIV-1 release by directly tethering virions to cells. Cell 139, 499–511, http://dx.doi.org/10.1016/j.cell.2009.08.039.

Phillips, R., Kondev, J., Theriot, J., Garcia, H., Chasan, B., 2010. Physical Biology of the Cell. Am. J. Phys. 78, 1230, http://dx.doi.org/10.1119/1.3459039.

Razooky, B.S., Weinberger, L.S., 2011. Mapping the architecture of the HIV-1 Tat circuit: a decision-making circuit that lacks bistability and exploits stochastic noise. Methods 53, 68–77, http://dx.doi.org/10.1016/j.ymeth.2010.12.006.

Rong, L., Perelson, A.S., 2009. Asymmetric division of activated latently infected cells may explain the decay kinetics of the HIV-1 latent reservoir and intermittent viral blips. Math. Biosci. 217, 77–87, http://dx.doi.org/10.1016/j.mbs.2008.10.006.

Reddy, B., Jhon, Y., 1999. Quantitative Intracellular Kinetics of HIV Type 1. AIDS Res. Hum. Retroviruses 15, 273–283.

Sadler, A.J., Latchoumanin, O., Hawkes, D., Mak, J., Williams, B.R.G., 2009. An antiviral response directed by PKR phosphorylation of the RNA helicase A. PLoS Pathog. 5, e1000311, http://dx.doi.org/10.1371/journal.ppat.1000311.

Sanghvi, V.R., Steel, L.F., 2012. RNA silencing as a cellular defense against HIV-1 infection: progress and issues. FASEB J 26, 3937–3945, http://dx.doi.org/10.1096/fj.12-210765.

Schröder, H.C., Ugarković, D., Wenger, R., Reuter, P., Okamoto, T., Müller, W.E.G., 1990. Binding of Tat protein to TAR region of human immunodeficiency virus type 1 blocks TAR-mediated activation of (2′--5′) oligoadenylate synthetase. AIDS Res. Hum. Retroviruses 6, 659–672.

Schwanhäusser, B., Busse, D., Li, N., Dittmar, G., Schuchhardt, J., Wolf, J., Chen, W., Selbach, M., 2011. Global quantification of mammalian gene expression control. Nature 473, 337–342, http://dx.doi.org/10.1038/nature10098.

Sisan, D.R., Halter, M., Hubbard, J.B., Plant, A.L., 2012. Predicting rates of cell state change caused by stochastic fluctuations using a data-driven landscape model. Proc. Nat. Acad. Sci. U.S.A (doi:10.1073/pnas.1207544109/-/DCSupplemental. www.pnas.org/cgi/doi/10.1073/pnas.1207544109).

Slice, L.W., Codner, E., Antelman, D., Holly, M., Wegrzynski, B., Wang, J., Toome, V., Hsu, M.C., Nalin, C.M., 1992. Characterization of recombinant HIV-1 Tat and its interaction with TAR RNA. Biochemistry 31, 12062–12068, http://dx.doi.org/10.1021/bi00163a014.

Strogatz, S.H., 1994. Nonlinear Dynamics and Chaos: With Applications to Physics, Biology, Chemistry, and Engineering, Studies in Nonlinearity Series. Perseus Books Group.

Tan, J., Pan, R., Qiao, L., Zou, X., Pan, Z., 2012. Modeling and dynamical analysis of virus-triggered innate immune signaling pathways. PLoS One 7, e48114, http://dx.doi.org/10.1371/journal.pone.0048114.

Tyagi, M., Kashanchi, F., 2012. New and novel intrinsic host repressive factors against HIV-1: PAF1 complex, HERC5 and others. Retrovirology 9, 19, http://dx.doi.org/10.1186/1742-4690-9-19.

Verdin, E., Paras, P., Van Lint, C., 1993. Chromatin disruption in the promoter of human immunodeficiency virus type 1 during transcriptional activation. EMBO J. 12, 3249–3259.

Weinberger, L.S., Burnett, J.C., Toettcher, J.E., Arkin, A.P., Schaffer, D. V, 2005. Stochastic gene expression in a lentiviral positive-feedback loop: HIV-1 Tat fluctuations drive phenotypic diversity. Cell122169–182http://dxdoi.org/10.1016/j.cell.2005.06.006.

Weinberger, L.S., Dar, R.D., Simpson, M.L., 2008. Transient-mediated fate determination in a transcriptional circuit of HIV. Nat. Genet. 40, 466–470, http://dx.doi.org/10.1038/ng.116.

Weinberger, L.S., Shenk, T., 2007. An HIV feedback resistor: auto-regulatory circuit deactivator and noise buffer. PLoS Biol. 5, e9, http://dx.doi.org/10.1371/journal.pbio.0050009.

Williams, S. a F., Greene, W.C., 2005. Host factors regulating post-integration latency of HIV. Trends Microbiol. 13, 137–139, http://dx.doi.org/10.1016/j.tim.2005.02.006.

Wu, L., 2012. SAMHD1: a new contributor to HIV-1 restriction in resting CD4+ T-cells. Retrovirology 9, 88, http://dx.doi.org/10.1186/1742-4690-9-88.

Wu, Y., 2004. HIV-1 gene expression: lessons from provirus and non-integrated DNA. Retrovirology 1, 13, http://dx.doi.org/10.1186/1742-4690-1-13.

Zack, J.A., Kim, S.G., Vatakis, D.N., 2013. HIV restriction in quiescent CD4+ T cells. Retrovirology 10, 37, http://dx.doi.org/10.1186/1742-4690-10-37.

Zhang, H., Yang, B., Pomerantz, R.J., Zhang, C., 2003. The cytidine deaminase CEM15 induces hypermutation in newly synthesized HIV-1 DNA. Nature, 424.

Zou, X., Xiang, X., Chen, Y., Peng, T., Luo, X., Pan, Z., 2010. Understanding inhibition of viral proteins on type I IFN signaling pathways with modeling and optimization. J. Theor. Biol. 265, 691–703, http://dx.doi.org/10.1016/j.jtbi.2010.05.001.